Study on methylene blue adsorption using cashew nut shell-based activated carbon

Hai D. Tran [a] [iD], Dinh Quan Nguyen [bc] * [iD]

a: Faculty of Environment, Ho Chi Minh University of Natural Resources and Environment, Ho Chi Minh city 700.000, Vietnam
b: Laboratory of Biofuel and Biomass Research, Faculty of Chemical Engineering, Ho Chi Minh City University of Technology (HCMUT), 268 Ly Thuong Kiet, District 10, Ho Chi Minh City 700.000, Vietnam
c: Vietnam National University Ho Chi Minh City, Linh Trung Ward, Thu Duc District, Ho Chi Minh City 700.000, Vietnam
* Corresponding author: ndquan@hcmut.edu.vn

This paper belongs to a Regular Issue.
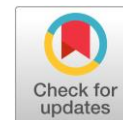
Abstract

Adsorption is a widely used technique for the treatment of wastewater containing dyes, which are pollutants that can have serious impacts on the aquatic ecosystems. In this work, activated carbon (AC) was prepared from cashew nut shell (CNS) and used to adsorb methylene blue (MB) from solution. The CNS AC was characterized by scanning electron microscopy, Fourier transform infrared spectroscopy, and nitrogen adsorption-desorption isotherms. The adsorption behavior of MB on CNS AC was investigated by varying the initial solution pH, adsorbent dosage, and initial MB concentration. The results showed that the CNS AC was effective for MB removal, with an adsorption capacity of 24.8 mg/g. The adsorption nature of MB onto the CNS AC surface was explored by analyzing the experimental data using isotherm and kinetic models. The Freundlich and Dubinin-Radushkevich (D-R) isotherm models showed good agreement with the experimental adsorption equilibrium results. The mean adsorption energy was found to be 22.4 kJ/mol, indicating chemical adsorption. The adsorption of MB on the CNS AC followed pseudo-second-order kinetics. This study demonstrates the potential application of CNS AC for MB removal.

Key findings

● The porous and rough surface of the CNS AC is rich in functional groups containing electron donors.

● The equilibrium of MB adsorption onto the CNS AC is in good agreement with the Freundlich and D-K isotherms.

● The adsorption kinetics correspond to the pseudo-second-order.

1. Introduction

Due to the hazardous nature of common dyes, such as their poor biodegradability, toxicity, stability, and coloration, the presence of dye pollutants in water has caused major environmental problems [1, 2]. Various techniques have been developed for dye removal, including biological treatment, chemical oxidation treatment, advanced oxidation processes, catalytic degradation, physical processes, or hybrid systems [3–6]. As a prominent method among physical processes, adsorption is considered economically feasible because of its highly removal-effective, operating-cost-effective, versatile, and available properties [7–9].

A large amount of CNS is being discharged in Vietnam, which poses a challenge for its management [10]. The high content of organic compounds in the CNS suggests that it should be considered as a raw material for the preparation of AC. The CNS AC exhibited a potential adsorbent for a variety of pollutants, including methylene blue (MB) [11–14], brilliant green dye [15], and Congo red dye [16]. The CNS AC can be prepared by chemical activation using $ZnCl_2$ [13], KOH [11, 14, 15], or H_3PO_4 [17]. Acid impregnation can be applied in the protocol of AC preparation to improve the adsorption capacity of AC via the formation of functional groups on the AC surface [18–21]. However, to the best of our knowledge, the CNS AC prepared after the

acid impregnation has not been fully investigated for its dye adsorption performance. This study aims to fill this gap by investigating the adsorption of MB on CNS AC that was prepared by HNO$_3$ activation. The influence of experimental parameters on MB removal was explored. The analysis of isotherm and kinetic results revealed the nature of MB adsorption on the CNS AC.

2. Materials and methods

2.1. Preparation and characterization of CNS AC

The CNS AC was prepared in two steps. First, the raw CNS, which had been mechanically squeezed to separate oil, was carbonized at 500 °C for 2 h to produce CNS charcoal. This charcoal was then crushed in a ball mill for 20 min. Second, the obtained charcoal was dispersed in an abundant amount of 0.5 M nitric acid (HNO$_3$) under ultrasonication for 15 minutes and then kept overnight. Solid particles were collected and neutralized by washing and filtrating through an 11-μm filter paper (Whatmann No. 1) with distilled water. The collected solid was dried at 100 °C for 1 h. The activation process was carried out at 800 °C for 30 min in an electric furnace, which was purged with nitrogen gas to create an inert atmosphere.

The functional groups and morphological structure of CNS AC were explored by Fourier transform infrared spectroscopy (FTIR) and scanning electron microscopy (SEM) using a Prisma E SEM system and an iS5 Nicolet FTIR spectrometer, respectively. Nitrogen adsorption-desorption isotherms were performed with a Nova 2200e® system (Quantachrome Instruments, USA) to determine the pore structure.

2.2. Preparation of MB solutions

A stock MB solution of 1000 ppm was prepared by dissolving 1.0 g of MB (Merck) in 1 L of distilled water. The MB solutions at the desired concentrations were obtained by diluting an appropriate volume of the stock solution. A solution of 0.1 M NaOH or 0.1 M HCl was used to adjust the pH of the MB solution.

2.3. Adsorption experiments

Batch adsorption experiments were conducted in a 500-ml Erlenmeyer flask, which was tightly attached with a silicone rubber stopper. The flask contained 350 ml of MB solution. A small glass tube (with an outer diameter of 4 mm) for sampling was inserted through this stopper. A magnetic stirrer was used to agitate the solution at 150 rpm.

The effects of solution pH, CNS AC dosage, and initial MB concentration on adsorption performance were investigated at a temperature of 300 K. To reach equilibrium adsorption, the experiment runs were carried out for 3 h. Then, samples were collected and filtered through a 0.45 μm membrane to determine the equilibrium concentration of MB.

For the kinetic study, MB adsorption was performed using the same procedures. The MB concentrations after different contact periods were measured by UV-Vis spectroscopy at wavelength of 664 nm using an Evolution™ 350 UV-Vis spectrophotometer.

Equation 1 was used to calculate the amount of adsorbed MB at time t, q_t (mg/g).

$$q_t = \frac{(C_o - C_t)V}{m} \qquad (1)$$

where, C_o and C_t are the concentrations of MB at initial and at any time t (mg/L), V is the volume of the solution (L), and m is the weight of CNS AC employed (g).

The adsorption experiment was triplicated to evaluate the accuracy of the results.

3. Results and Discussion

3.1. Morphology of CNS AC

The CNS AC surface has a porous and rough morphology, as shown in Figure 1. This morphology is characterized by large and interconnected open channels, which were formed by the decomposition and evaporation of volatile matter during thermal treatment [22]. This structure is proposed to facilitate the transfer of MB molecules from solution to adsorption sites [23], resulting in a fast adsorption rate.

3.2. Analysis of porous structure

Nitrogen adsorption and desorption measurements were used to characterize the porous structure of CNS AC. The hysteresis loop in the relative pressure range of 0.3–1.0 (Figure 2) is a sign of Type IV isotherm according to the IUPAC classification, indicating the presence of mesopores in the CNS AC structure [24, 25]. This is further supported by the BJH pore size distribution (inset in Figure 2), which shows that the pore diameters are less than 4 nm, with micropores (< 2 nm) being the dominant pore type. The specific surface area was calculated to be 472 m²/g using the Brunauer-Emmett-Teller method.
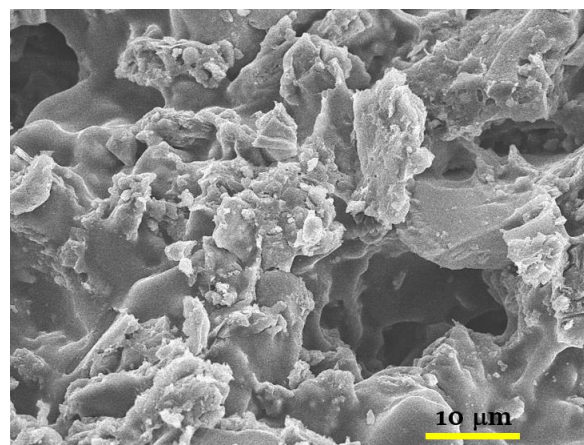

Figure 1 SEM image of the CNS AC.

3.3. Characterization of the surface chemistry

The FTIR spectrum (Figure 3) displayed characteristic peaks, which provide information on the functional groups on the surface of CNS AC. The band at 3400 cm^{-1} indicates the O–H stretching vibration in water molecules. The C–H sp^3 stretching bond of alkane was assigned as the cause of the appearance of the peak at 2921 cm^{-1} [26, 27]. The sign of C–H aliphatic stretching was illustrated by a band at 2787 cm^{-1} [28]. The vibration of C≡C stretching in alkyne groups was reflected by a band at 2285 cm^{-1}. The bands at 1632 and 731 cm^{-1} correspond to C=O and C–O stretching in aromatic carboxyl, phenolic ester, and conjugated ketonic structures [26]. C–O vibration in alcohol groups is related to a band at 1158 cm^{-1}. The peak at 1050 cm^{-1} identified C–C bending in the aromatic ring [29]. The presence of the groups containing π bonds (C≡C, C=O) and the Lewis base groups (C=O, C–O) is proposed to promote the interaction of cationic MB molecules with the CNS AC surface [30–32].

4. Batch adsorption studies

4.1. Effect of solution pH

The pH of the solution plays an important role in the adsorption of dyes [32]. As shown in Figure 4, the MB removal and q_e increased with increasing solution pH from 1 to 5. This is because (1) the functional groups on the CNS AC surface become more negatively charged as the pH value increases [33], and (2) MB is deprotonated to form a positively charged species if the solution pH is higher than the pKa of MB (5.85) [34]. As a result, the electrostatic attraction between the MB molecules and the CNS AC surface is enhanced with increasing solution pH, leading to improved MB adsorption. However, at solution pH values above 5, the competitive adsorption of hydroxide ions (OH$^-$) with MB molecules begins to occur, leading to a gradual decrease in MB removal [35]. Therefore, the subsequent adsorption experiments were performed at pH 5, where the maximum MB removal and q_e were achieved.

4.2. Effect of CNS AC dosage

The adsorption of MB onto CNS AC was investigated at different adsorbent dosages (0.5, 1.0, 1.5, and 2.0 g). As shown in Figure 5, MB removal increased with increasing adsorbent dosage, reaching a plateau at 1.5 g. This is because the higher adsorbent dosage provides more adsorptive sites for MB molecules to bind to [36]. At 2.0 g of the CNS AC dosage, the MB removal was not significantly higher than at 1.5 g. The adsorption capacity decreased from 42.6 to 14.1 mg/g as the CNS AC dosage increased from 0.5 to 2.0 g. The excess of adsorptive sites at higher dosages led to an unsaturated adsorption surface, resulting in a decrease in adsorption capacity [37]. This trend was previously reported for MB adsorption on various biomass-based adsorbents [38–40].

4.3. Effect of initial MB concentration

The initial dye concentration affects the dye adsorption performance, which is related to the interfacial process [41]. As shown in Figure 6, when the initial MB concentration was increased from 20 to 90 mg/L, the MB removal decreased from 95.7 to 41.3%, while the adsorption capacity increased from 12.8 to 24.8 mg/g.
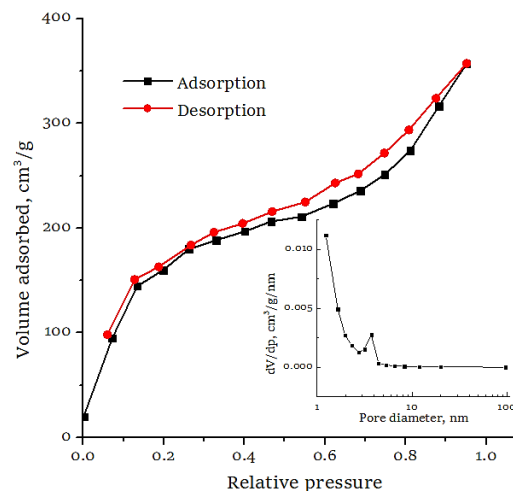

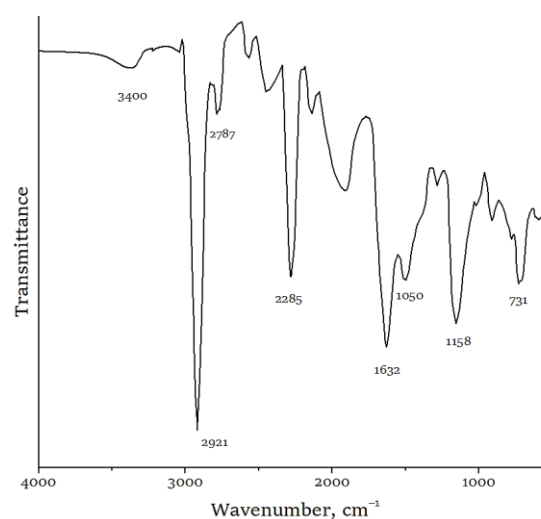**Figure 2** Nitrogen adsorption-desorption isotherms (the inset: pore-size distribution).

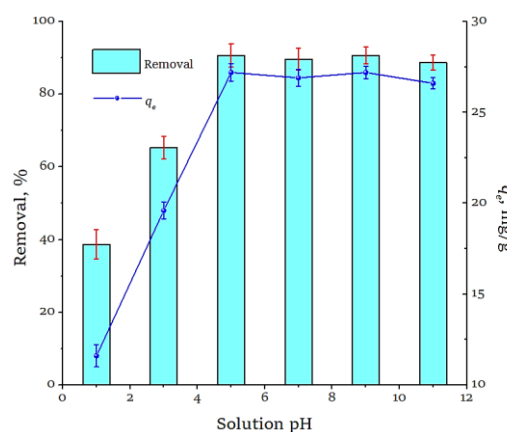
Figure 3 FTIR spectrum of the CNS AC.

Figure 4 Effect of initial pH (conditions: C_0 = 30 mg/L, m = 1 g, t = 3 hours).

The higher the MB concentration, the greater the driving force and collision probability between MB cations and adsorptive sites [38, 41]. However, increasing the initial MB concentration causes a denser MB accumulation on the CNS AC surface, which leads to faster saturation of adsorptive sites [42]. Therefore, the adsorption capacity increased with increasing initial MB concentration, while the MB removal changed in the opposite direction. This behavior is consistent with previous reports [43, 44].

4.4. Adsorption isotherms

The nature and mechanism of the interaction between MB molecules and the CNS AC surface can be explored by an adsorption isotherm study [45]. In this study, the equilibrium data were analyzed according to the Langmuir, Freundlich, and Dubinin-Radushkevich (D-R) isotherms, which were mathematically expressed as equation 2–4 [46].

$$q_e = \frac{q_{max}K_L C_e}{1 + K_L C_e} \qquad (2)$$

$$q_e = K_F C_e^{1/n} \qquad (3)$$

$$q_e = q_{max} e^{-K_{DR}\varepsilon^2} \qquad (4)$$

$$\varepsilon = RT\left(1 + \frac{1}{C_e}\right) \qquad (5)$$

where C_e and q_e are the MB concentration (mg/L) and adsorption capacity (mg/g) at equilibrium, respectively, q_{max} is the theoretical maximum adsorption capacity (mg/g), K_L is the Langmuir isotherm constant (L/mg), K_F is the Freundlich isotherm constant (mg/g (mg/L)^n), n represents the adsorption intensity, K_{DR} is the activity coefficient related to the mean sorption energy (mol²/J²), ε is the Polyani potential (J²/mol²), R = 8.314 (J/mol/K) is the gas constant, and T = 300 K is the solution temperature.

The constant parameters for the selected isotherm models were determined by nonlinear fitting to the experimental data and are presented in Table 1. Figure 7 shows the relationship between the q_e and the C_e from the experiment (desired points) and regression (solid plots).

The closeness between the isotherm model and experimental results was evaluated using the correlation coefficient, R^2. The Langmuir isotherm model assumes a monolayer coverage of adsorbate onto a homogenous adsorbent surface [47]. The R^2 value of 0.8980 (Table 1) for the Langmuir model indicates that it is unsatisfactory for describing the equilibrium data obtained. This suggests that the adsorption of MB onto the CNS AC surface occurs in multilayers. This may be due to the presence of electron donors via functional groups.

The Freundlich and D-R isotherm models provide better fits with the experimental data compared to the Langmuir isotherm model, as indicated by higher R^2 values in Table 1. Equilibrium data following Freundlich implies a multilayer adsorption of the adsorbate onto a heterogeneous adsorbent surface where there is a non-

uniform distribution of the adsorption energy and affinities [45, 48]. The Freundlich isotherm model yielded a K_F value of 14.7 mg/g (mg/L)^n, which is higher than previous report [49]. The high K_F value reflects a high adsorption capacity. The n value was determined to be 7.3 according to the Freundlich isotherm model. For n > 1, the greater the n value, the greater the adsorption intensity [45]. This resulted in a favorable adsorption for increasing the adsorption capacity. The K_F and n values are consistent in explaining the mechanism of MB adsorption onto the CNS AC.
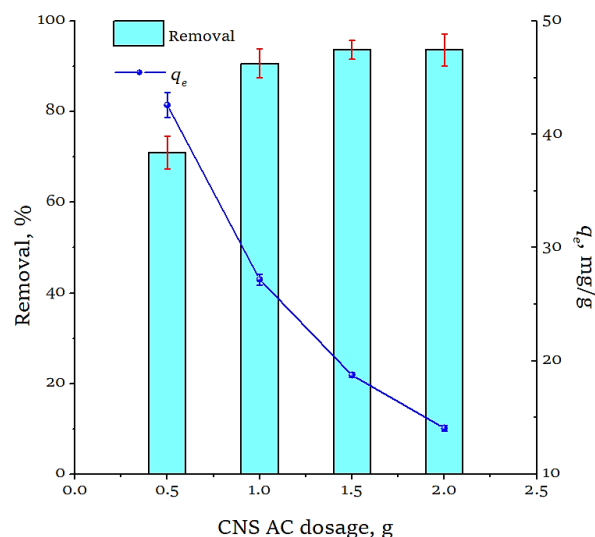
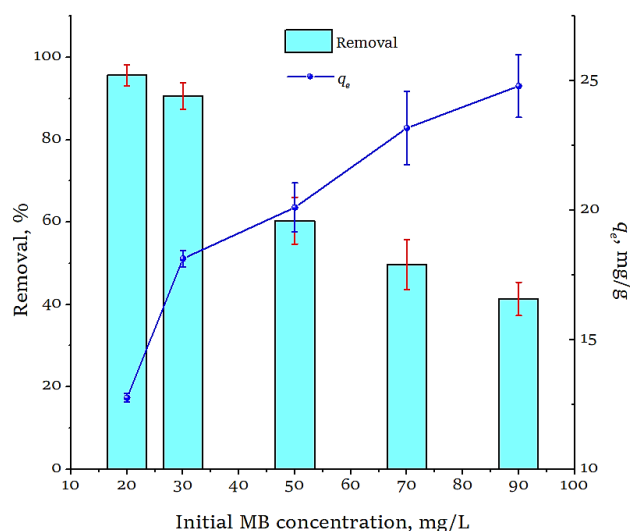**Figure 5** Effect of CNS AC dosage (conditions: C_o = 30 mg/L, pH 5, t = 3 hours).

Figure 6 Effect of initial concentration of MB (conditions: m = 1.5 g, pH 5, t = 3 h).

Table 1 The calculated parameters for the selected isotherm models.

Isotherm model	R^2	Calculated parameter
Langmuir	0.8980	q_{max} = 23.28
		K_L = 1.32
Freundlich	0.9295	K_F = 14.14
		n = 7.27
Dubinin-Radushkevich	0.9316	q_{max} = 39.52
		K_{DR} = 10.39×10^{-10}

The D-R isotherm considers micropores filled with adsorbate molecules and sorption energy at the adsorbent surface according to a Gaussian distribution [49]. As shown in the inset of Figure 2, the range of pore-size diameters in CNS AC is less than 4 nm, which is close to the effective diameter of the MB molecule (length of 1.45 nm, width of 0.95 nm) [50]. This allows MB molecules to transfer into the porous matrix and fill micropores. The good fit of the experimental data to the D-R isotherm (R^2 = 0.932) supports this hypothesis. According to equation 6, the mean adsorption energy (E) can be calculated to be 22.4 kJ/mol, which is higher than the threshold for chemical adsorption of 20 kJ/mol, implying the chemical adsorption of MB onto CNS AC [51, 52].

$$E = \frac{1}{\sqrt{2K_{DR}}} . \tag{6}$$

4.5. Kinetic studies

The dynamics of MB adsorption on CNS AC were investigated by nonlinear fitting of the experimental kinetic data with three common kinetic models: the pseudo-first-order (PFO), pseudo-second-order (PSO), and intra-particle diffusion (W-M) models. These models were expressed by equations 7–9 [53].

$$q_t = q_e \left(1 - e^{-k_1 t}\right) \tag{7}$$

$$q_t = \frac{q_e^2 k_2 t}{1 + k_2 q_e t} \tag{8}$$

$$q_t = k_{W-M} t^{0.5} + c \tag{9}$$

where q_t (mg/g) is the amount adsorbed of MB at contact time t, q_e (mg/g) is the predicted adsorption capacity at equilibrium; k_1 (1/min), k_2 (g/mg/min), and k_{W-M} (g/mg/min$^{0.5}$) are rate constants of PFO, PSO, and W-M, respectively; and c (mg/g) represents the contribution of molecular diffusion through the boundary layer.

The dependence of the adsorbed MB amount on the contact time is shown in Figure 8. The experimental results (desired points) indicate that the MB was rapidly adsorbed onto the CNS AC in the first 60 min. This is due to the large BM concentration gradient between the bulk solution and the CNS AC surface.

The obtained kinetic parameters are presented in Table 2. A comparison of the R^2 values from the simulation of the three kinetic models suggests that the PSO model is the best fitting model to describe the kinetic behavior of MB adsorption on CNS AC. This indicates that the adsorption rate is controlled by the chemical interaction between MB and the adsorptive sites on the CNS AC surface [42, 54]. The calculated adsorption capacity for MB (18.74 mg/g) according to the PSO model was in good agreement with the experiment result (18.65 mg/g). The adsorption mechanism of MB onto CNS AC was investigated in a consensus of kinetic and isothermal analyses.

5. Limitations

Experiments on competitive adsorption and applicability for real textile wastewater have not been conducted.

6. Conclusion

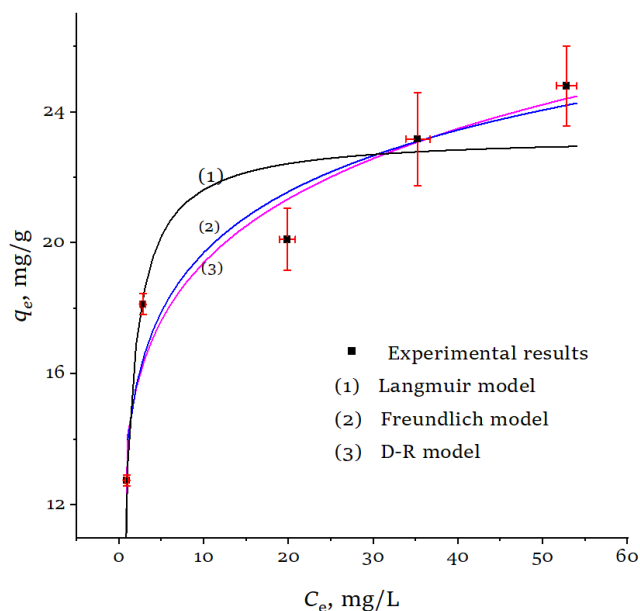In this work, Vietnamese CNS was activated with nitric acid to synthesize CNS AC.

Figure 7 Isotherm plots for MB adsorption onto the CNS AC (conditions: m = 1.5 g, pH 5, t = 3 h).
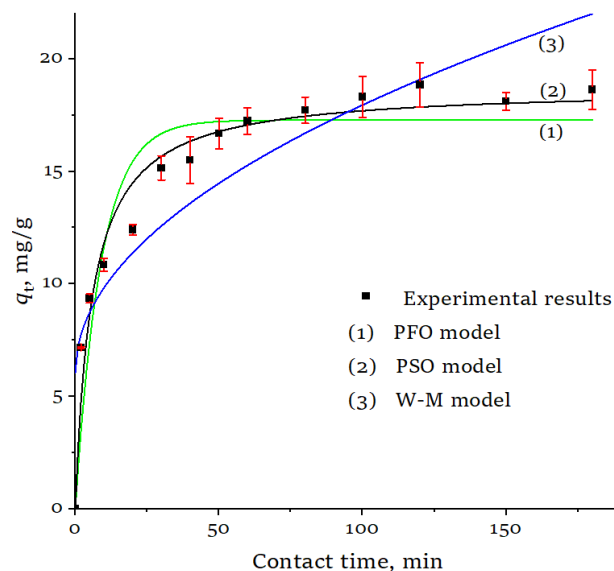

Figure 8 Adsorption kinetics of MB on CNS AC (C$_o$ = 30 mg/L, m = 1.5 g, pH 5).

Table 2 The calculated parameters for the selected kinetic models.

Kinetic model	R^2	Calculated parameter
PFO	0.9014	q_e = 17.29
		k_1 = 0.11
PSO	0.9636	q_e = 18.74
		k_2 = 9.10×10^{-3}
W-M	0.8023	c = 6.07
		k_{W-M} = 1.19

The obtained CNS AC exhibited a porous structure with functional groups containing oxygen or π-bonds, which were advantageous for the interaction with cationic molecules. The adsorption of MB on the CNS AC was performed at different solution pH values, adsorbent dosages, and initial MB concentrations. The experimental equilibrium data was consistent with Freundlich and D-R models, suggesting that the adsorption of MB onto CNS AC is a favorable process that occurs in multilayers on a heterogeneous surface. The mean adsorption energy was found to be 22.4 kJ/mol, confirming the chemisorption process. The kinetic results followed the pseudo-second-order kinetic model. The results provide valuable insights into the adsorption mechanism of MB on CNS AC, which can be used to optimize the adsorption process and improve the removal efficiency.

● Supplementary materials

No supplementary materials are available.

● Funding

● Acknowledgments

● Author contributions

Conceptualization: D.Q.N.
Data curation: H.D.T.
Investigation: H.D.T.
Methodology: D.Q.N., H.D.T.
Validation: D.Q.N.
Writing – original draft: H.D.T.
Writing – review & editing: D.Q.N.

● Conflict of interest

The authors declare no conflict of interest.

● Additional information

Author IDs:

Hai D. Tran, Scopus ID 56226812800;
Dinh Quan Nguyen, Scopus ID 15123160800;

Websites:

Ho Chi Minh University of Natural Resources and Environment, http://www.hcmunre.edu.vn/;
Ho Chi Minh City University of Technology, http://www.hcmut.edu.vn/;
Vietnam National University Ho Chi Minh City, https://vnuhcm.edu.vn/.

References

1. Khan I, Saeed K, Zekker I, Zhang B, Hendi AH, Ahmad A, Ahmad S, Zada N, Ahmad H, Shah LA. Review on methylene blue: Its properties, uses, toxicity and photodegradation. Water. 2022;14(2):242. doi:10.3390/w14020242

2. Lellis B, Fávaro-Polonio CZ, Pamphile JA, Polonio JC. Effects of textile dyes on health and the environment and bioremediation potential of living organisms. Biotechnol Res Innov. 2019;3(2):275–290. doi:10.1016/j.biori.2019.09.001

3. Beya CL, Kanwugu ON, Ivantsova MN. Modern biotechnological methods in wastewater treatment: a review. Chimica Techno Acta. 2022;9(2S):202292S3. doi:10.15826/chimtech.2022.9.2.S3

4. Javaid R, Qazi UY. Catalytic oxidation process for the degradation of synthetic dyes: An overview. Int J Environ Res Public Health. 2019;16(11):2066. doi:10.3390/ijerph16112066

5. Nguyet PN, Watari T, Hirakata Y, Hatamoto M, Yamaguchi T. Adsorption and biodegradation removal of methylene blue in a down-flow hanging filter reactor incorporating natural adsorbent. Environ Technol. 2021;42(3):410–418. doi:10.1080/09593330.2019.1629636

6. Nachiyar CV, Rakshi A, Sandhya S, Jebasta NBD, Nellore J. Developments in treatment technologies of dye-containing effluent: A review. Case Stud Chem Environ Eng. 2023;7:100339. doi:10.1016/j.cscee.2023.100339

7. Aragaw TA, Bogale FM. Biomass-based adsorbents for removal of dyes from wastewater: a review. Front Environ Sci. 2021;9:764958. doi:10.3389/fenvs.2021.764958

8. Yardımcı B, Kanmaz N. An effective-green strategy of methylene blue adsorption: sustainable and low-cost waste cinnamon bark biomass enhanced via MnO_2. J Environ Chem Eng. 2023;11(3):110254. doi:10.1016/j.jece.2023.110254

9. Hızal J, Kanmaz N, Yılmazoğlu M. Adsorption efficiency of sulfonated poly (ether ether ketone)(sPEEK) as a novel low-cost polymeric adsorbent for cationic organic dyes removal from aqueous solution. J Mol Liq. 2021;322:114761. doi:10.1016/j.molliq.2020.114761

10. Nam NH, Anh KD, Truc LGT, Ha TA, Ha VTT. Pyrolysis of cashew nut shell: A parametric study. Vietnam J Chem. 2020;58(4):506–511. doi:10.1002/vjch.202000015

11. Subramaniam R, Ponnusamy SK. Novel adsorbent from agricultural waste (cashew NUT shell) for methylene blue dye removal: Optimization by response surface methodology. Water Resour Ind. 2015;11:64–70. doi:10.1016/j.wri.2015.07.002

12. Thang NH, Khang DS, Hai TD, Nga DT, Tuan PD. Methylene blue adsorption mechanism of activated carbon synthesised from cashew nut shells. RSC Adv. 2021;11:26563–26570. doi:10.1039/D1RA04672A

13. Spagnoli AA, Giannakoudakis DA, Bashkova S. Adsorption of methylene blue on cashew nut shell based carbons activated with zinc chloride: The role of surface and structural parameters. J Mol Liq. 2017;229:465–471. doi:10.1016/j.molliq.2016.12.106

14. Kumar PS, Ramalingam S, Sathishkumar K. Removal of methylene blue dye from aqueous solution by activated carbon prepared from cashew nut shell as a new low-cost adsorbent. Korean J Chem Eng. 2011;28:149–155. doi:10.1007/S11814-010-0342-0

15. Samiyammal P, Kokila A, Pragasan LA, Rajagopal R, Sathya R, Ragupathy S, Krishnakumar M, Reddy VRM. Adsorption of brilliant green dye onto activated carbon prepared from cashew nut shell by KOH activation: Studies on equilibrium isotherm. Environ Res. 2022;212:113497. doi:10.1016/j.envres.2022.113497

16. Kumar PS, Ramalingam S, Senthamarai C, Niranjanaa M, Vijayalakshmi P, Sivanesan S. Adsorption of dye from aqueous solution by cashew nut shell: Studies on equilibrium isotherm, kinetics and thermodynamics of interactions. Desalination 2010;261(1–2):52–60. doi:10.1016/j.desal.2010.05.032

17. Geczo A, Giannakoudakis DA, Triantafyllidis K, Elshaer MR, Rodríguez-Aguado E, Bashkova S. Mechanistic insights into

acetaminophen removal on cashew nut shell biomass-derived activated carbons. Environ Sci Pollut Res. 2021;28:58969–58982. doi:10.1007/s11356-019-07562-0

18. Kim MI, Bai BC. Effect of nitric acid treatment on the pitch properties and preparation of activated carbon. Carbon Lett. 2022;32:99–107. doi:10.1007/s42823-021-00256-z

19. Farnane M, Machrouhi A, Abdennouri M, Tounsadi H, Rais Z, Qourzal S, Barka N. Optimization of Carob shells biomass activation by nitric acid for heavy metals sequestration from contaminated water. Biointerface Res Appl Chem. 2021;12(5):5941–5952. doi:10.33263/briac125.59415952

20. Fillaeli A, Kristianingrum S, Siswani E, Fatimah S. Synthesis activated carbon of screw-pine leaves by HNO₃ and its properties. In J Phys Conf Ser. 2019;012001. doi:10.1088/1742-6596/1156/1/012001

21. Neme I, Gonfa G, Masi C. Activated carbon from biomass precursors using phosphoric acid: A review. Heliyon. 2022;8(12):e11940. doi:10.1016/j.heliyon.2022.e11940

22. Torres J, Nogueira F, Silva M, Lopes J, Tavares T, Ramalho T, Corrêa A. Novel eco-friendly biocatalyst: soybean peroxidase immobilized onto activated carbon obtained from agricultural waste. RSC Adv. 2017;7(27):16460–16466. doi:10.1039/C7RA01309D

23. Ma F, Ding S, Ren H, Liu Y. Sakura-based activated carbon preparation and its performance in supercapacitor applications. RSC Adv. 2019;9(5):2474–2483. doi:10.1039/C8RA09685F

24. Tsai J-H, Lee T-Y, Chiang H-L. Nitrogen adsorption and characteristics of iron, cobalt, and nickel oxides impregnated on SBA-15 mesoporous silica. Nanomater. 2023;13(6):1015. doi:10.3390/nano13061015

25. Kanmaz N, Buğdaycı M, Demirçivi P. Investigation on structural and adsorptive features of BaO modified zeolite powders prepared by ball milling technique: Removal of tetracycline and various organic contaminants. Microporous Mesoporous Mater. 2023;354:112566. doi:10.1016/j.micromeso.2023.112566

26. Li X, Qiu J, Hu Y, Ren X, He L, Zhao N, Ye T, Zhao X. Characterization and comparison of walnut shells-based activated carbons and their adsorptive properties. Adsorp Sci Technol. 2020;38(9–10):450–463. doi:10.1177/0263617420946

27. Kanmaz N, Buğdaycı M, Demirçivi P. Solvent-free mechanochemical synthesis of TiO₂-ethyl cellulose biocomposite for adsorption of tetracycline and organic dyes. J Mol Liq. 2023;378:121643. doi:10.1016/j.molliq.2023.121643

28. Moyo M, Nyamhere G, Sebata E, Guyo U. Kinetic and equilibrium modelling of lead sorption from aqueous solution by activated carbon from goat dung. Desalin Water Treat. 2016;57(2):765–775. doi:10.1080/19443994.2014.968217

29. Cuhadaroglu D, Uygun OA. Production and characterization of activated carbon from a bituminous coal by chemical activation. Afr J Biotechnol. 2008;7(20):3703–3710. English. Available from: https://www.ajol.info/index.php/ajb/article/view/59416, Accessed on 20 Oct 2008.

30. Ghaffar A, Younis MN. Interaction and thermodynamics of methylene blue adsorption on oxidized multi-walled carbon nanotubes. Green Process Synth. 2015;4(3):209–217. doi:10.1515/gps-2015-0009

31. Sáenz-Alanís CA, García-Reyes RB, Soto-Regalado E, García-González A. Phenol and methylene blue adsorption on heat-treated activated carbon: Characterization, kinetics, and equilibrium studies. Adsorp Sci Technol. 2017;35(9–10):789–805. doi:10.1177/0263617416684517

32. Rabadanova A, Abdurakhmanov M, Gulakhmedov R, Shuaibov A, Selimov D, Sobola D, Částková K, Ramazanov S, Orudzhev F. Piezo-, photo-and piezophotocatalytic activity of electro-spun fibrous PVDF/CTAB membrane. Chimica Techno Acta. 2022;9(4):20229420. doi:10.15826/chimtech.2022.9.4.20

33. Hongo T, Moriura M, Hatada Y, Abiko H. Simultaneous methylene blue adsorption and pH neutralization of contaminated water by rice husk ash. ACS Omega. 2021;6(33):21604–21612. doi:10.1021/acsomega.1c02833

34. Zein R, Purnomo JS, Ramadhani P, Alif MF, Putri CN. Enhancing sorption capacity of methylene blue dye using solid waste of lemongrass biosorbent by modification method. Arab J Chem. 2023;16(2):104480. doi:10.1016/j.arabjc.2022.104480

35. Zhang J, Cai D, Zhang G, Cai C, Zhang C, Qiu G, Zheng K, Wu Z. Adsorption of methylene blue from aqueous solution onto multiporous palygorskite modified by ion beam bombardment: Effect of contact time, temperature, pH and ionic strength. Appl Clay Sci. 2013;83–84:137–143. doi:10.1016/j.clay.2013.08.033

36. Amode JO, Santos JH, Md. Alam Z, Mirza AH, Mei CC. Adsorption of methylene blue from aqueous solution using untreated and treated (Metroxylon spp.) waste adsorbent: equilibrium and kinetics studies. Int J Ind Chem. 2016;7:333–345. doi:10.1007/s40090-016-0085-9

37. Han R, Zou W, Yu W, Cheng S, Wang Y, Shi J. Biosorption of methylene blue from aqueous solution by fallen phoenix tree's leaves. J Hazard Mater. 2007;141(1):156–162. doi:10.1016/j.jhazmat.2006.06.107

38. Mosoarca G, Vancea C, Popa S, Gheju M, Boran S. *Syringa vulgaris* leaves powder a novel low-cost adsorbent for methylene blue removal: Isotherms, kinetics, thermodynamic and optimization by Taguchi method. Sci Rep. 2020;10:17676. doi:10.1038/s41598-020-74819-x

39. Kujawska J, Wasag H. Biochar: a low-cost adsorbent of methylene blue from aqueous solutions. In J Phy: Conf Ser. 2021 Nov 23–26; Lublin, Poland - Lviv, Ukraine. 012002. doi:10.1088/1742-6596/1736/1/012002

40. Fito J, Abewaa M, Mengistu A, Angassa K, Ambaye AD, Moyo W, Nkambule T. Adsorption of methylene blue from textile industrial wastewater using activated carbon developed from *Rumex abyssinicus* plant. Sci Rep. 2023;13:5427. doi:10.1038/s41598-023-32341-w

41. Al-Ghouti MA, Al-Absi RS. Mechanistic understanding of the adsorption and thermodynamic aspects of cationic methylene blue dye onto cellulosic olive stones biomass from wastewater. Sci Rep. 2020;10:15928. doi:10.1038/s41598-020-72996-3

42. Eren Z, Acar FN. Adsorption of Reactive Black 5 from an aqueous solution: equilibrium and kinetic studies. Desalination 2006;194(1–3):1–10. doi:10.1016/j.desal.2005.10.022

43. Etim U, Umoren S, Eduok U. Coconut coir dust as a low cost adsorbent for the removal of cationic dye from aqueous solution. J Saudi Chem Soc. 2016;20:S67–S76. doi:10.1016/j.jscs.2012.09.014

44. Mousavi SA, Mahmoudi A, Amiri S, Darvishi P, Noori E. Methylene blue removal using grape leaves waste: optimization and modeling. Appl Water Sci. 2022;12:112. doi:10.1007/s13201-022-01648-w

45. Kalam S, Abu-Khamsin SA, Kamal MS, Patil S. Surfactant adsorption isotherms: A review. ACS Omega. 2021;6(48):32342–32348. doi:10.1021/acsomega.1c04661

46. Wang J, Guo X. Adsorption isotherm models: Classification, physical meaning, application and solving method. Chemosphere. 2020;258:127279. doi:10.1016/j.chemosphere.2020.127279

47. Langmuir I. The adsorption of gases on plane surfaces of glass, mica and platinum. J Am Chem Soc. 1918;40(9):1361–1403. doi:10.1021/ja02242a004

48. Freundlich H. Über die adsorption in lösungen. Z fur Phys Chem. 1907;57U(1):385–470. doi:10.1515/zpch-1907-5723

49. Banerjee S, Chattopadhyaya M. Adsorption characteristics for the removal of a toxic dye, tartrazine from aqueous solutions by a low cost agricultural by-product. Arab J Chem. 2017;10:S1629–S1638. doi:10.1016/j.arabjc.2013.06.005

50. Jia P, Tan H, Liu K, Gao W. Removal of methylene blue from aqueous solution by bone char. Appl Sci. 2018;8(10):1903. doi:10.3390/app8101903

51. Tahir S, Rauf N. Removal of a cationic dye from aqueous solutions by adsorption onto bentonite clay. Chemosphere 2006;63(11):1842–1848.
doi:10.1016/j.chemosphere.2005.10.033

52. SenthilKumar P, Ramalingam S, Abhinaya R, Kirupha SD, Vidhyadevi T, Sivanesan S. Adsorption equilibrium, thermodynamics, kinetics, mechanism and process design of zinc (II) ions onto cashew nut shell. Can J Chem Eng. 2012;90(4):973–982. doi:10.1002/cjce.20588

53. Wang J, Guo X. Adsorption kinetic models: Physical meanings, applications, and solving methods. J Hazard Mater. 2020;390:122156. doi:10.1016/j.jhazmat.2020.122156

54. Chen B, Yue W, Zhao H, Long F, Cao Y, Pan X. Simultaneous capture of methyl orange and chromium (VI) from complex wastewater using polyethylenimine cation decorated magnetic carbon nanotubes as a recyclable adsorbent. RSC Adv. 2019;9(9):4722–4734. doi:10.1039/C8RA08760A